

R.A. 1375

UNCLASSIFIED

~~CONFIDENTIAL~~

RM No. L7F17

JUL 1 1947

NACA

RESEARCH MEMORANDUM

for the

Bureau of Aeronautics, Navy Department

FLIGHT-TEST EVALUATION OF THE LONGITUDINAL STABILITY AND CONTROL
CHARACTERISTICS OF 0.5-SCALE MODELS OF THE FAIRCHILD LARK
PILOTLESS-AIRCRAFT CONFIGURATION

STANDARD CONFIGURATION WITH WING FLAPS DEFLECTED 60° AND
MODEL HAVING TAIL IN LINE WITH WINGS

TEST NO. NACA 2387

By

David G. Stone

Langley Memorial Aeronautical Laboratory
Langley Field, Va.

Restriction/

Classification

Cancelled

This document contains information which, if disclosed, would reveal the national defense of the United States to an unauthorized person. Information so classified may be imparted only to persons in the military and naval services of the United States, appropriate civilian officers and employees of the Federal Government who have a legitimate interest therein, and to United States citizens of known loyalty and discretion who of necessity must be informed thereof.

dition
lated
Act,
the
to an
law.

NATIONAL ADVISORY COMMITTEE FOR AERONAUTICS

WASHINGTON

JUN 25 1947

UNCLASSIFIED

LANGLEY MEMORIAL AERONAUTICAL
LABORATORY
Langley Field, Va.

~~CONFIDENTIAL~~

CLASSIFICATION CANCELLED

Authority NACA RA 2956 Date 3/2/55
By JMA 3/21/55 Soc

UNCLASSIFIED



3 1176 01436 3551

NACA RM No. L7F17

NATIONAL ADVISORY COMMITTEE FOR AERONAUTICS

RESEARCH MEMORANDUM

for the

Bureau of Aeronautics, Navy Department

FLIGHT-TEST EVALUATION OF THE LONGITUDINAL STABILITY AND CONTROL
CHARACTERISTICS OF 0.5-SCALE MODELS OF THE FAIRCHILD LARK
PILOTLESS-AIRCRAFT CONFIGURATION

STANDARD CONFIGURATION WITH WING FLAPS DEFLECTED 60° AND
MODEL HAVING TAIL IN LINE WITH WINGS

TED NO. NACA 2387

By David G. Stone

SUMMARY

Flight tests were conducted at the Flight Test Station of the Pilotless Aircraft Research Division at Wallops Island, Va., to determine the longitudinal control and stability characteristics of 0.5-scale models of the Fairchild Lark pilotless aircraft with the tail in line with the wings and with the horizontal wing flaps deflected 60° . The data were obtained by the use of a telemeter and by radar tracking.

Placing the tail in line with the wings results in a considerable reduction in the effectiveness of the longitudinal trimming control. This configuration is statically stable with large increases in the longitudinal stability occurring above a Mach number of 0.7. The model exhibited dynamic stability throughout the speed range. The aerodynamic lag of the trimming control encountered in the tail-in-line configuration would make angle-of-attack stabilization very difficult.

Deflecting the horizontal wing flaps 60° with the tail interdigitated with the wings results in a reduction in the effectiveness of the trimming control as compared to a flap deflection of 15° . Deflecting the horizontal wing flaps 60° produces considerable increase in the static longitudinal stability at high Mach numbers. Similarly, with flaps deflected 60° the aerodynamic lag of the trimming control would make angle-of-attack stabilization difficult.

~~CONFIDENTIAL~~

UNCLASSIFIED

[REDACTED]

INTRODUCTION

The NACA was requested by the Bureau of Aeronautics, Navy Department, to make flight tests of the Fairchild Lark pilotless-aircraft configuration to evaluate the longitudinal stability and control characteristics at high subsonic speeds in order to predict the behavior of the full-scale aircraft. In order to obtain this information 0.5-scale models, externally geometrically similar to the Fairchild Lark, were constructed and flown at the Flight Test Station of the Pilotless Aircraft Research Division at Wallops Island, Va. The results reported herein pertain to the longitudinal characteristics of the following configurations: (1) model with the tail surfaces in line with the wings and wing flaps not deflected, and (2) model of the standard configuration (dihedral of tail surfaces 45°) with the wing flaps deflected 60° .

The full-scale Fairchild Lark is flown at constant angle of attack. The lift increments for maneuvering are gained by deflection of the horizontal wing flaps, and the longitudinal control surfaces are used only as trimmers. In these model tests the control surfaces produced angle of attack, but tests with various wing-flap deflections provided data for an evaluation of the effectiveness of the trimming control function. The models were flown with a programmed flicker-type deflection of the longitudinal trimming control surfaces.

SYMBOLS

t	time from launching, seconds
M	free-stream Mach number
p	free-stream static pressure, pounds per square foot
q	free-stream dynamic pressure, pounds per square foot $\left(\frac{\gamma}{2}\rho M^2\right)$
H	free-stream total pressure, pounds per square foot
C_N	normal-force coefficient
C_C	chord-force coefficient
$\frac{dC_m}{d\alpha}$	rate of change of pitching-moment coefficient with angle of attack, per degree
$\frac{dC_L}{d\alpha}$	rate of change of lift coefficient with angle of attack, per degree

[REDACTED]

$\frac{\Delta \left(\frac{a_n}{g} \right)}{\Delta \delta_e}$	rate of change of normal acceleration with elevator deflection, per degree
P	period of oscillation, seconds
I_y	moment of inertia about Y-axis, slug-feet ²
W	weight of model, pounds
S	horizontal wing area, 2.725 square feet
c	wing chord, 0.883 foot
a_l	longitudinal acceleration, feet per second per second
a_n	normal acceleration, feet per second per second
g	acceleration of gravity, 32.2 feet per second per second
δ_f	deflection of horizontal wing flaps, degrees
δ_e	deflection of rudder elevators or elevators, degrees (trailing edge down is positive)
γ	specific heat ratio; value taken, 1.4

MODELS AND APPARATUS

The simplified 0.5-scale models used in this investigation were externally geometrically similar to the full-scale Lark (KAQ-1) of the Pilotless Plane Division of the Fairchild Engine and Airplane Corporation. Descriptions of the 0.5-scale Lark models are given in references 1 and 2.

Model with Tail in Line with Wings

Figure 1 presents the general arrangement of the model with the tail surfaces in the same plane as the wings. A photograph of this model with rocket motor and blast tube is shown in figure 2. The tail-in-line tests were accomplished by rotating the tail section, by fastening the vertical control surfaces at 0° deflection, and by connecting the servosystem to the horizontal control surfaces which were then elevators. For this flight the elevators were

deflected from approximately -11° to 10° in programmed movement to give a flicker-type operation. This control-surface motion was in operation before the model left the launcher and all during the flight. For this flight the wing flaps were not deflected.

The model was ground-launched without a booster on a zero-length launcher set at an angle of 45° from level. A photograph of the model on the launcher is shown in figure 3.

The general specifications of the model as compared to the full-scale aircraft are given in table I.

Standard Configuration Model

Figure 4 presents the general arrangement of the model representing the standard configuration. A photograph of this model with rocket motor and blast tube is shown in figure 5. This flight was made with the horizontal wing flaps deflected 60° , and the rudder-elevators were deflected from approximately -9° to 6° in a programmed flicker-type operation. A detail photograph of the horizontal wing flap deflected down 60° is shown in figure 6.

This model was ground-launched without a booster on a zero-length launcher set at an angle of 30° from level. A photograph of the model on the launcher is shown in figure 7. A photograph of the model in flight as it left the launcher is shown in figure 8.

The general specifications of the model as compared to the full-scale aircraft are given in table I.

Apparatus

The data from the flights were obtained by the use of a telemeter, CW Doppler radar, and photography. The four-channel telemeters gave continuous signals of the longitudinal acceleration, normal acceleration, impact pressure, and control-surface deflection. The impact-pressure record from the telemeter was reduced to Mach number by the following equation:

$$M^2 = \frac{2}{\gamma - 1} \left[\left(1 - \frac{H - P}{H} \right)^{\frac{\gamma - 1}{\gamma}} - 1 \right]$$

where p was taken as the pressure at sea level at the time of the tests. Since the models reached an altitude of only about 500 feet during the high-speed region, no large errors in M are introduced by taking p constant. The velocity of sound for the tail-in-line tests was 1136 feet per second and for the standard-configuration tests was 1142 feet per second.

The normal-acceleration factor and the normal-force coefficient were based on a linear variation with time of the wing loading from the take-off condition to the burnout condition.

RESULTS AND DISCUSSION

Time-History Records

Tail-in-line model. - A time history of the flight of a 0.5-scale model Lark with the tail in line with the wings and $\delta_f = 0^\circ$ is presented in figure 9. The total elapsed flight time was 40.8 seconds. Only the first 8 seconds of the flight are presented since no change in the recorded flight characteristics was noted until the compressed air for the servosystem was expended a few seconds later. The maximum speed obtained corresponds to a Mach number of 0.87, occurs at a time of 3.86 seconds after launching, and coincides with the burning out of the rocket motor. The dashed Mach number curve was obtained by integration of the longitudinal acceleration with the initial point at $t = 2.4$ where the data from the total head and radar check exactly. After $t = 3.8$ the total-head channel failed to record properly, and the recording time of the radar was expended at $t = 3.6$.

Referring to figure 9, it may be seen that the normal acceleration, with the usual short-period oscillations, followed the deflection of the elevators throughout the speed range. Positive normal accelerations of $7g$ and negative accelerations of $3g$ were obtained for elevator deflections of approximately -10° and 11° , respectively. No reversal of the normal acceleration was experienced for the speed range encountered. The low maximum velocity as compared with that shown in reference 1 can be attributed to poor rocket thrust as indicated by $a_1 \approx 7g$ as compared with $a_1 \approx 9g$ in previous tests.

Figure 10 presents the variation of normal-force coefficient with Mach number for the power-on flight period. Figure 11 presents curves of chord-force and normal-force coefficients for the power-off decelerating part of the flight. At times where $C_N = 0$ the C_C may be said to be equivalent to drag coefficient; hence at $t = 4.79$ ($M = 0.81$) the drag coefficient is 0.069, decreasing to 0.033 at $t = 7.56$ ($M = 0.73$).

Standard configuration model ($\delta_f = 60^\circ$). - A time history of the flight of a 0.5-scale model Lark of standard configuration flaps deflected 60° is presented in figure 12. The total elapsed flight time was 17.9 seconds. As determined from visual and photographic observation, the model began a slow roll near $t = 1.8$ indicating that the right wing flap loosened resulting in unknown deflections, and near $t = 7.0$ the right wing flap broke off causing a severe roll. Further record conversion beyond the time the flap broke off was considered unnecessary. The maximum speed obtained corresponds to a Mach number of 0.91, occurs at $t = 3.78$, and coincides with the burning out of the rocket motor. The dashed Mach number curve was obtained by integration of the longitudinal acceleration. For this flight the total-head channel and the Doppler radar failed to record properly.

Referring to figure 12, it may be seen that the normal acceleration, with the usual short-period oscillations, followed the deflection of the rudder-elevators throughout the speed range. Although the right wing flap had loosened, normal accelerations of $30g$ were obtained for a rudder-elevator deflection of -9° . Also, after the flap loosened, considerable waviness occurred in the longitudinal acceleration curve.

Figure 13 presents the variation of normal-force coefficient with Mach number for the power-on flight period. Figure 14 presents curves of chord-force and normal-force coefficients for the power-off decelerating part of the flight.

Longitudinal Stability

Evaluations of the static longitudinal stability were obtained by analysis of the short-period oscillation induced by the abrupt movement of the elevators as described in reference 3. The following equation was used to determine the rate of change of pitching-moment coefficient with angle of attack:

$$\frac{dC_m}{d\alpha} = -\frac{4\pi^2 I_y}{57.3P^2 q S c}$$

The variations of center of gravity and moment of inertia are included in the computation of $\frac{dC_m}{d\alpha}$.

The values of $\frac{dC_m}{d\alpha}$ obtained are for the model-flight center-of-gravity locations which for the tail-in-line configuration varied

from 18.86- to 18.51-percent chord and for the standard configuration varied from 19.34- to 18.29-percent chord as the rocket motor burned out.

The values of the period P determined from figures 9 and 12 are presented in figure 15 to show the variation of the period of oscillation with Mach number. The scatter of the test points on figure 15 indicates the amount of error in determining P . Considerable scatter is shown for the $\delta_f \approx 60^\circ$ case. This may be due to loosening of the flap.

Figure 16 presents the static longitudinal stability, as computed using the above equation, as a function of Mach number. These curves indicate that as M increases, the stability increases greatly for both configurations. With the tail in line with the wings, the static stability is less at low Mach numbers but increases faster and is greater as M increases as compared with the tail interdigitated with the wings. For the case of $\delta_f \approx 60^\circ$ at high values of C_N the stability does not increase as fast with increasing Mach number as at low values of C_N .

By taking the value of the slope of the lift curve $\frac{dC_L}{d\alpha}$ to be 0.08 (reference 3), and also including the variation of the center of gravity, the neutral points were computed for these conditions. The neutral points, of course, do not include the probable changes in $\frac{dC_L}{d\alpha}$ with Mach number. The variations of the neutral points for the tail-in-line model ($\delta_f = 0^\circ$) and the standard-configuration model ($\delta_f \approx 60^\circ$) with M are given in figure 17. Again the increase in stability is indicated by the large rearward movement of the neutral point as M increases above 0.70.

Longitudinal Control

On the full-scale Lark the tail control surfaces are used for trimming the aircraft only, whereas the lift increments are gained by wing-flap deflections or all-movable wings. In these model tests the control surfaces produced changes of angle of attack, but tests with various wing-flap deflections provided the data for an evaluation of the ability of the control surfaces to trim the airplane at high lifts. The ability of the longitudinal control surfaces to produce normal accelerations is presented in figure 18 as a plot of normal-acceleration factor against Mach number.

The normal-acceleration factor $\frac{\Delta \left(\frac{a_n}{g} \right)}{\Delta \delta_e} \left(\frac{V}{S} \right)$ was determined by the total change in $\frac{a_n}{g}$ for the total change in δ_e . This method of

determining the normal-acceleration factor eliminates the need for determining the δ_e required for $\frac{a_n}{g} = 0$ as was required for computation of the normal-acceleration factor in reference 1. The values of the normal-acceleration factor neglect the effects of the difference between normal force and lift force, and the rate of change of flight path with time. The maximum variation of center-of-gravity locations between models is approximately 2-percent chord. The difference due to power-on in the $\delta_f \approx 60^\circ$ case is probably caused by thrust misalignment with center of gravity. In order to obtain the normal accelerations produced per degree of elevator deflection for any desired wing loading, divide the normal-acceleration factor by the desired wing loading. For example, at $M = 0.75$ and $\frac{W}{S} = 110$, the following comparisons may be made:

δ_f	0.5-scale model			Full-scale aircraft		
	W/S (lb/sq ft)	c.g., percent chord	$\frac{a_n}{g}$ per δ_e	W/S (lb/sq ft)	c.g., percent chord	$\frac{a_n}{g}$ per δ_e
0°	38.9	16.64	-0.86	110	16.64	-0.30
15°	36.6	19.81	-1.95	110	19.81	-.65
60°	39.2	18.60	-1.20	110	18.60	-.43
0° tail lined up	38.4	18.60	-.26	110	18.60	-.09

It is evident that placing the tail in line with the wings results in an appreciable loss in the ability of the elevators to produce normal accelerations. Also, wing-flap deflections of 60° show a reduction in $\frac{a_n}{g}$ per δ_e as compared to $\delta_f = 15^\circ$ up to $M \approx 0.8$. It may be noted that at $M = 0.75$ the longitudinal stability is approximately the same for the tail-in-line and tail-interdigitated tests; therefore, the change in $\frac{a_n}{g}$ per δ_e must be due to a reduction in the effectiveness of the trimming control. Also, since the stability is less for the $\delta_f \approx 60^\circ$ configuration, this again indicates a reduction in control effectiveness for trimming. This reduction in control effectiveness may be attributed to wing-wake effects upon the tail.

Also shown in figures 9 and 12, the production of normal acceleration lags the application of control deflection. For the test of the tail-in-line model, the lag in the produced normal acceleration is of the order of 0.10 to 0.15 second after application of

the control. For the model with flaps deflected 60° the lag is approximately 0.10 second. These lag times may be compared to values of 0 to 0.05 second shown in references 1 and 2 for the standard model with $\delta_f = 0^\circ$ and 15° . This lag in the effectiveness of the elevators may be due again to wake interference from the wing. The magnitude of this aerodynamic lag is such as to seriously complicate the internal stability of an autopilot servosystem.

CONCLUSIONS

The flight tests to determine the longitudinal stability and control characteristics with the tail in line with the wings ($\delta_f = 0^\circ$) and with the horizontal wing flaps deflected down 60° for the Fairchild Lark pilotless aircraft were conducted at the Flight Test Station of the Pilotless Aircraft Research Division at Wallops Island, Va. From the results of the flight tests, the following general conclusions are indicated:

Placing the tail in line with the wings results in a considerable reduction in the effectiveness of the longitudinal trimming control. This configuration is statically stable with large increases in the longitudinal stability occurring above $M \approx 0.7$. The model exhibited dynamic stability throughout the speed range. The aerodynamic lag of the trimming control encountered in the tail-in-line configuration would make angle-of-attack stabilization very difficult.

Deflecting the horizontal wing flaps 60° with the tail interdigitated with the wings results in a reduction in the effectiveness of the trimming control as compared to $\delta_f = 15^\circ$ up to $M \approx 0.80$. Deflecting the flaps 60° produces a considerable increase in static longitudinal stability at high Mach numbers. Similarly, with flaps deflected 60° , the aerodynamic lag of the trimming control would make angle-of-attack stabilization difficult.

Langley Memorial Aeronautical Laboratory
National Advisory Committee for Aeronautics
Langley Field, Va.

David G. Stone
David G. Stone
Aeronautical Engineer

Approved:

Robert R. Gilruth
Robert R. Gilruth

Chief of Pilotless-Aircraft Research Division

REFERENCES

1. Stone, David G., and Mitcham, Grady L.: Flight-Test Evaluation of the Longitudinal Stability and Control Characteristics of 0.5-Scale Models of the Fairchild Lark Pilotless-Aircraft Configuration. Model with Wing Flaps Not Deflected - TED No. NACA 2387. NACA MR No. L6H22, Bur. Aero., 1946.
2. Stone, David G.: Flight-Test Evaluation of the Longitudinal Stability and Control Characteristics of 0.5-Scale Models of the Fairchild Lark Pilotless-Aircraft Configuration. Model with Wing Flaps Deflected 15° - TED No. NACA 2387. NACA RM No. L6J28a, Bur. Aero., 1946.
3. Stone, David G.: Flight-Test Evaluation of the Longitudinal Stability and Control Characteristics of 0.5-Scale Models of the Fairchild Lark Pilotless-Aircraft Configuration. Static Longitudinal Stability of Models with Wing Flap Deflections of 0° and 15° - TED No. NACA 2387. NACA RM No. L6L17a, Bur. Aero., 1946.

TABLE I.- GENERAL SPECIFICATIONS

~~CONFIDENTIAL~~

Item	Full-scale aircraft	0.5-scale models	
		Tail in line	Standard
Fuselage:			
Over-all length, in.	164	82	82
Maximum diameter, in.	17	8.5	8.5
Wings:			
Aspect ratio	3.49	3.49	3.49
Total span, in.	74	37	37
Chord (constant), in.	21.2	10.6	10.6
Angle of incidence, deg	0	0	0
Dihedral, deg	0	0	0
Sweep, deg	0	0	0
Airfoil section:			
Horizontal wing	NACA 16-209	NACA 16-209	NACA 16-209
Vertical wing	NACA 16-009	NACA 16-009	NACA 16-009
Wing area (per pair including fuselage), sq ft	10.9	2.725	2.725
Tail surfaces:			
True span, in.	48	24	24
Chord (constant), in.	15.4	7.7	7.7
Angle of incidence, deg	0	0	0
Dihedral, deg	45	0	45
Sweep, deg	0	0	0
Airfoil section	NACA 16-008	NACA 16-008	NACA 16-008
Horizontal area (including fuselage), sq ft	Total projected 7.25	1.283	Total projected 1.813
Propulsion:			
Type rocket	Liquid	Powder	Powder
Approximate thrust, lb	600	1000	1200
Approximate thrust, sec	220	3.9	3.8
Center-of-gravity location, percent chord	20	{ Take-off 18.86 Burnout 18.51	{ Take-off 19.34 Burnout 18.29
Weight, lb	1060	{ Take-off 125.4 Burnout 97.9	{ Take-off 127.1 Burnout 99.6
Wing loading, lb/sq ft	110	{ Take-off 46.0 Burnout 35.9	{ Take-off 46.6 Burnout 36.6
Moment of inertia about Y-axis, slug-ft²	221 (approx.)	{ Take-off 8.30 Burnout 7.85	{ Take-off 9.30 Burnout 8.85

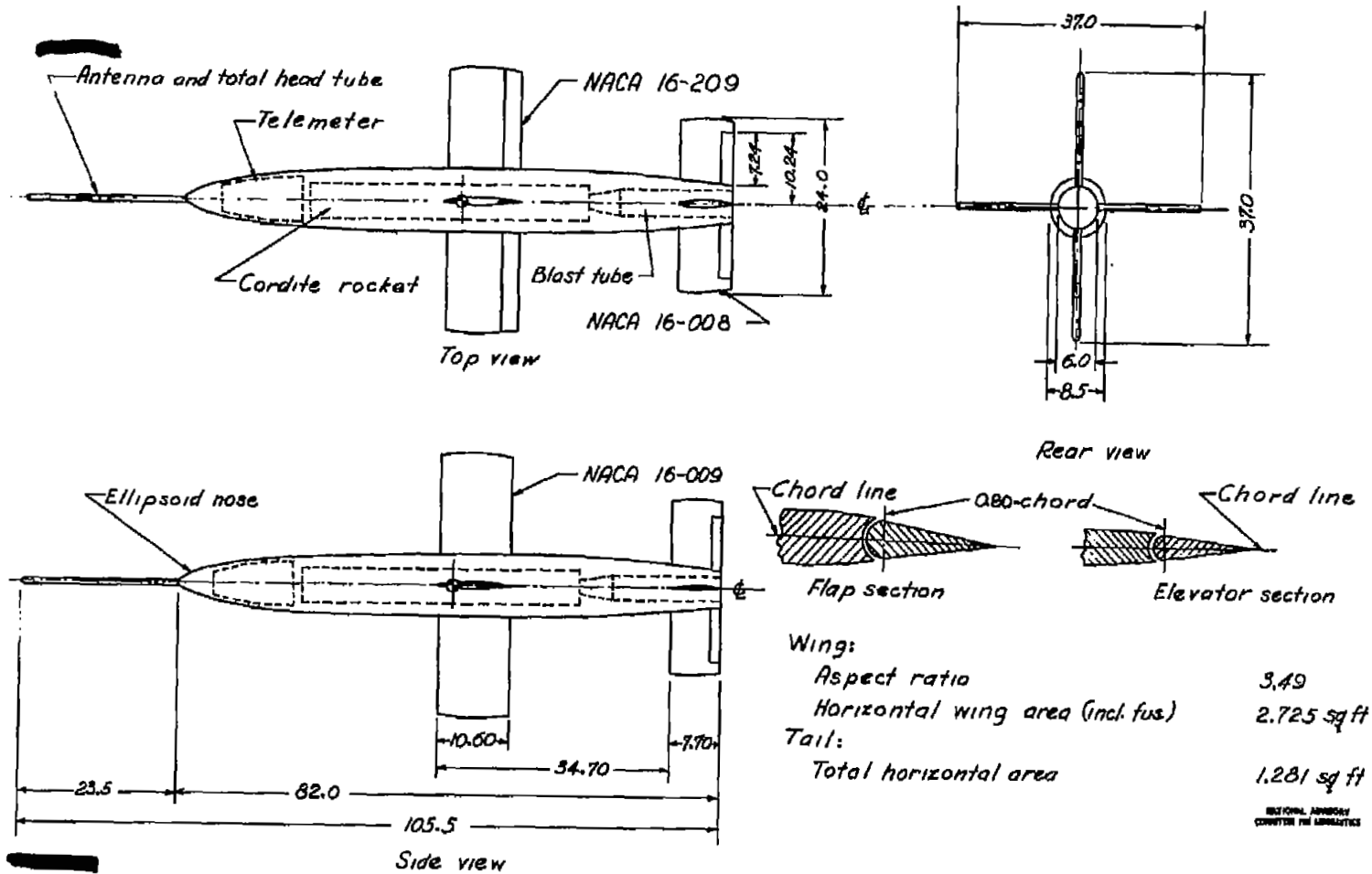


Figure 1.-General arrangement of 0.5-scale model of Fairchild Lark Pilotless Aircraft with tail in line with wing; all dimensions in inches; all wing and tail tips are solids of revolution.

CONFIDENTIAL

NACA RM No. L7F17

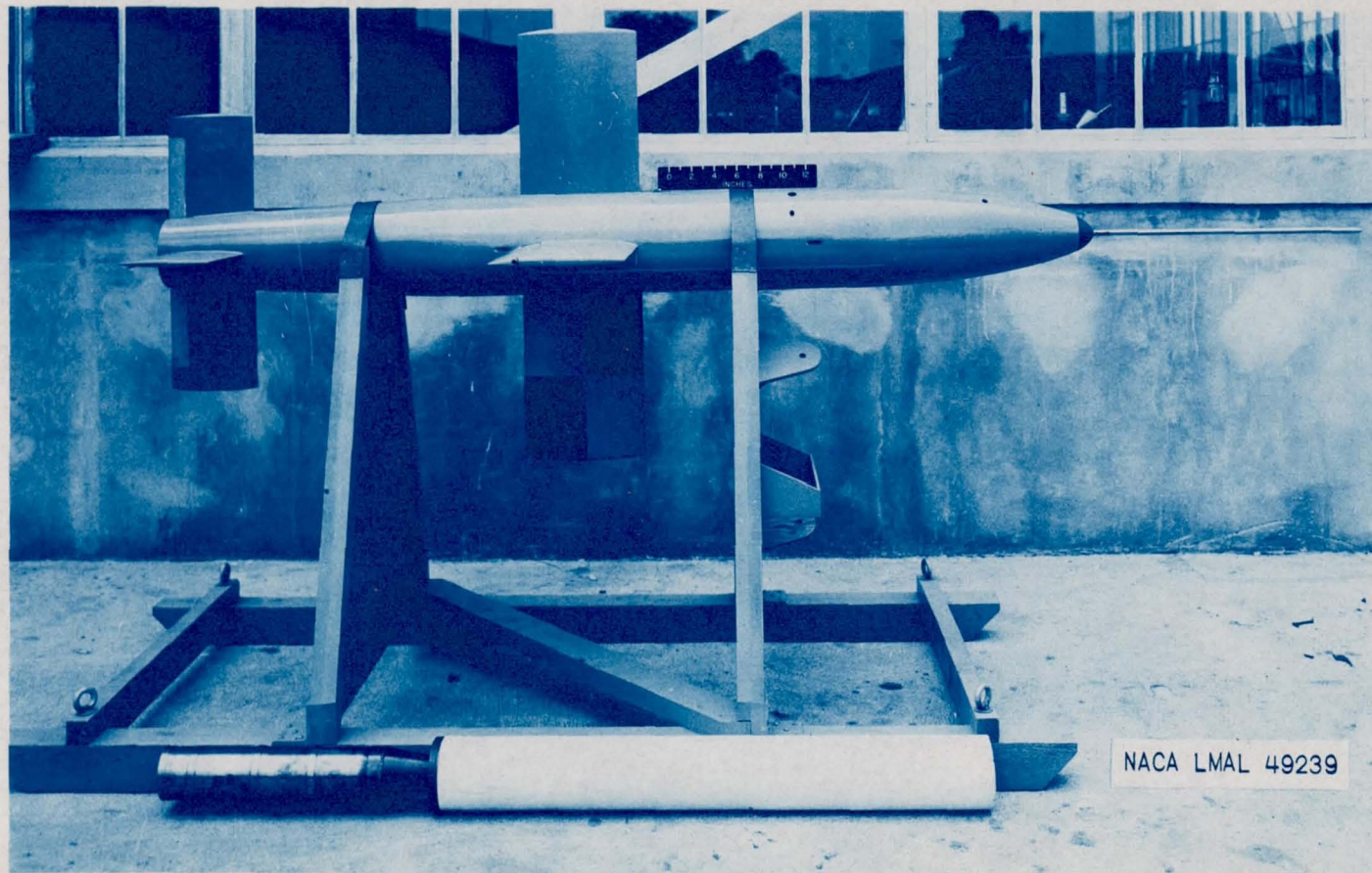


Figure 2.- Photograph of tail-in-line model with rocket motor and blast tube.

CONFIDENTIAL

NATIONAL ADVISORY COMMITTEE FOR AERONAUTICS
LANGLEY MEMORIAL AERONAUTICAL LABORATORY - LANGLEY FIELD, VA.

Fig. 2

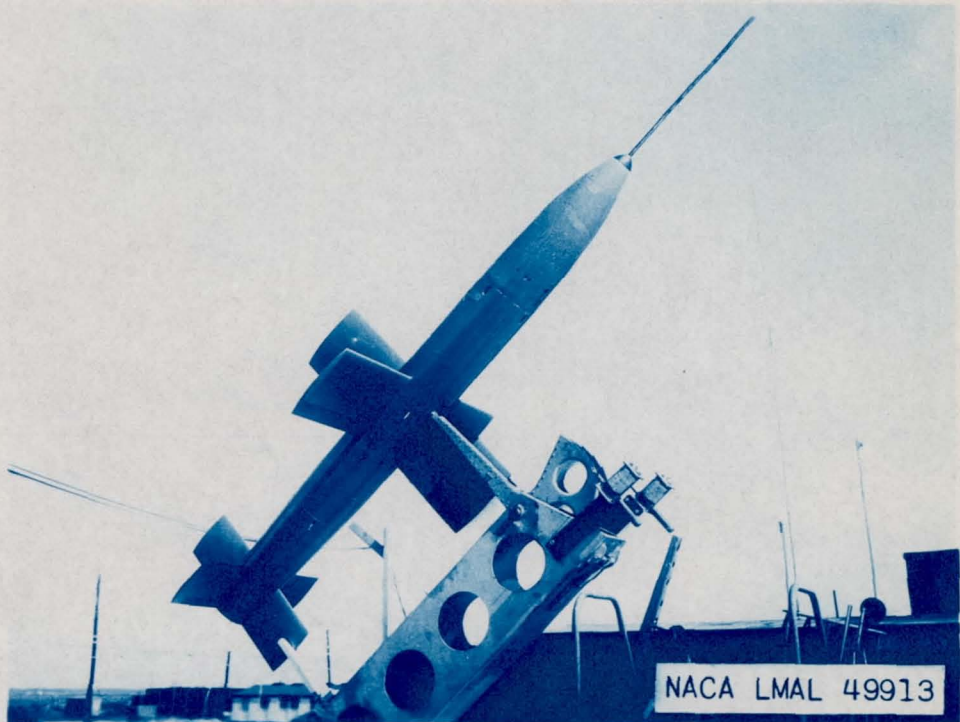


Figure 3.- Tail-in-line model on launcher.

CONFIDENTIAL

NATIONAL ADVISORY COMMITTEE FOR AERONAUTICS
LANGLEY MEMORIAL AERONAUTICAL LABORATORY - LANGLEY FIELD, VA.

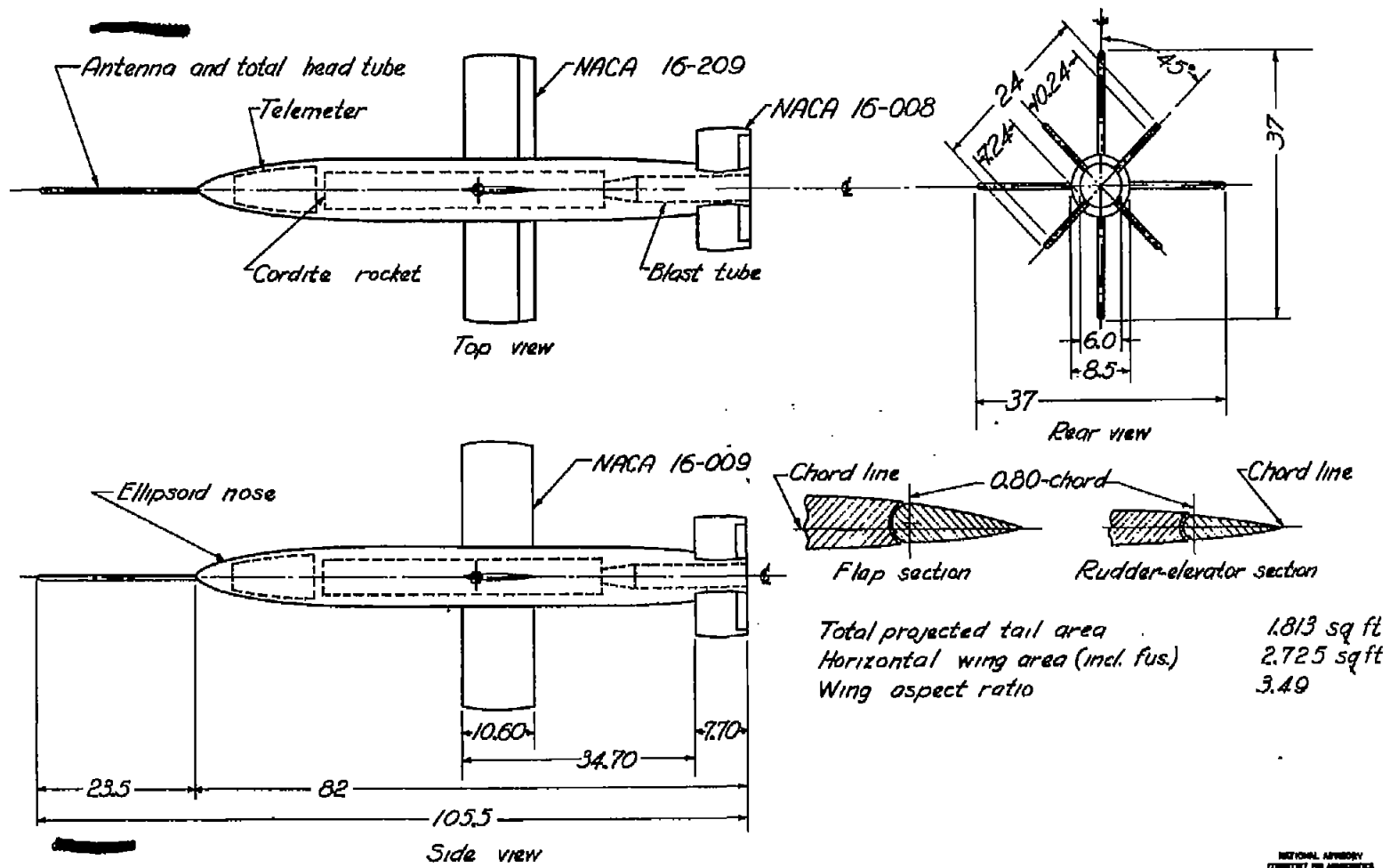
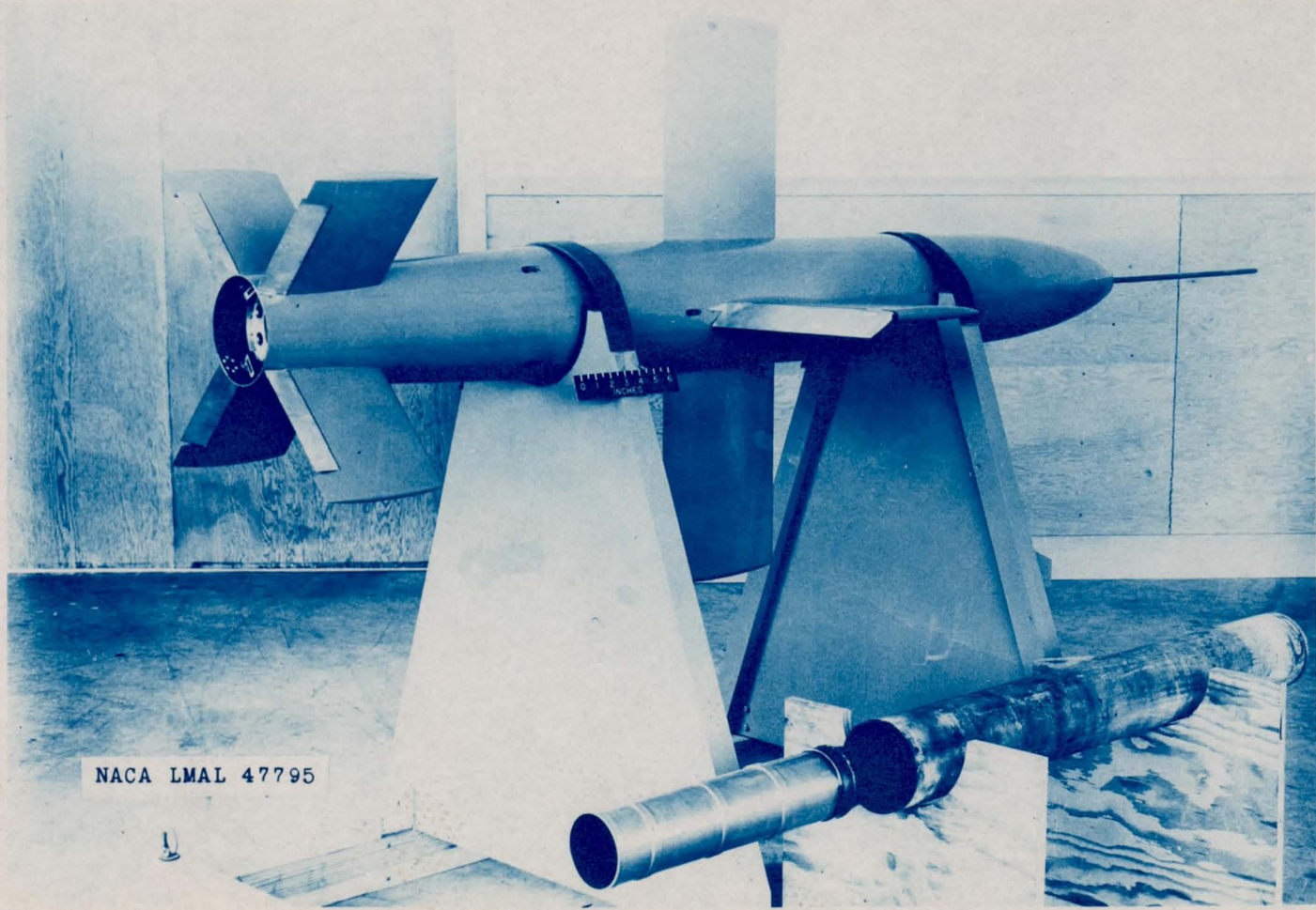


Figure 4.- General arrangement of 0.5-scale model of Fairchild Lark Pilotless Aircraft ; all dimensions in inches ; all wing and tail tips are solids of revolution.



CONFIDENTIAL

NACA RM No. L7F17



NACA LMAL 47795

Figure 5.- Photograph of standard configuration model with rocket motor and blast tube.

CONFIDENTIAL

NATIONAL ADVISORY COMMITTEE FOR AERONAUTICS
LANGLEY MEMORIAL AERONAUTICAL LABORATORY - LANGLEY FIELD, VA

Fig. 5

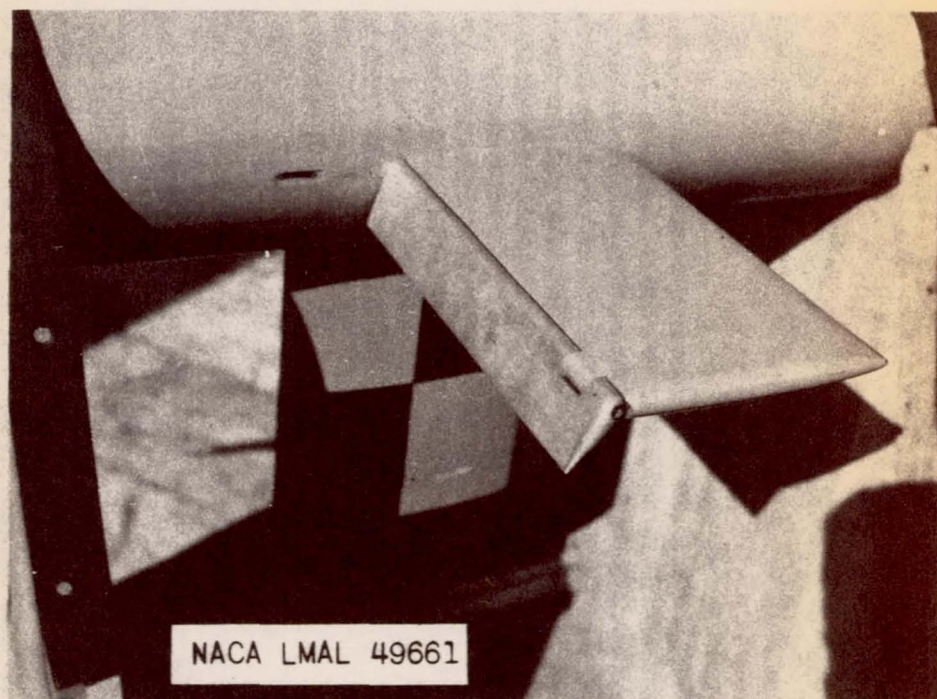


Figure 6.- Photograph of horizontal wing flap deflected 60° on standard configuration model.

CONFIDENTIAL

NATIONAL ADVISORY COMMITTEE FOR AERONAUTICS
LANGLEY MEMORIAL AERONAUTICAL LABORATORY - LANGLEY FIELD, VA



Figure 7.- Standard-configuration model on launcher.

CONFIDENTIAL

NATIONAL ADVISORY COMMITTEE FOR AERONAUTICS
LANGLEY MEMORIAL AERONAUTICAL LABORATORY - LANGLEY FIELD, VA.

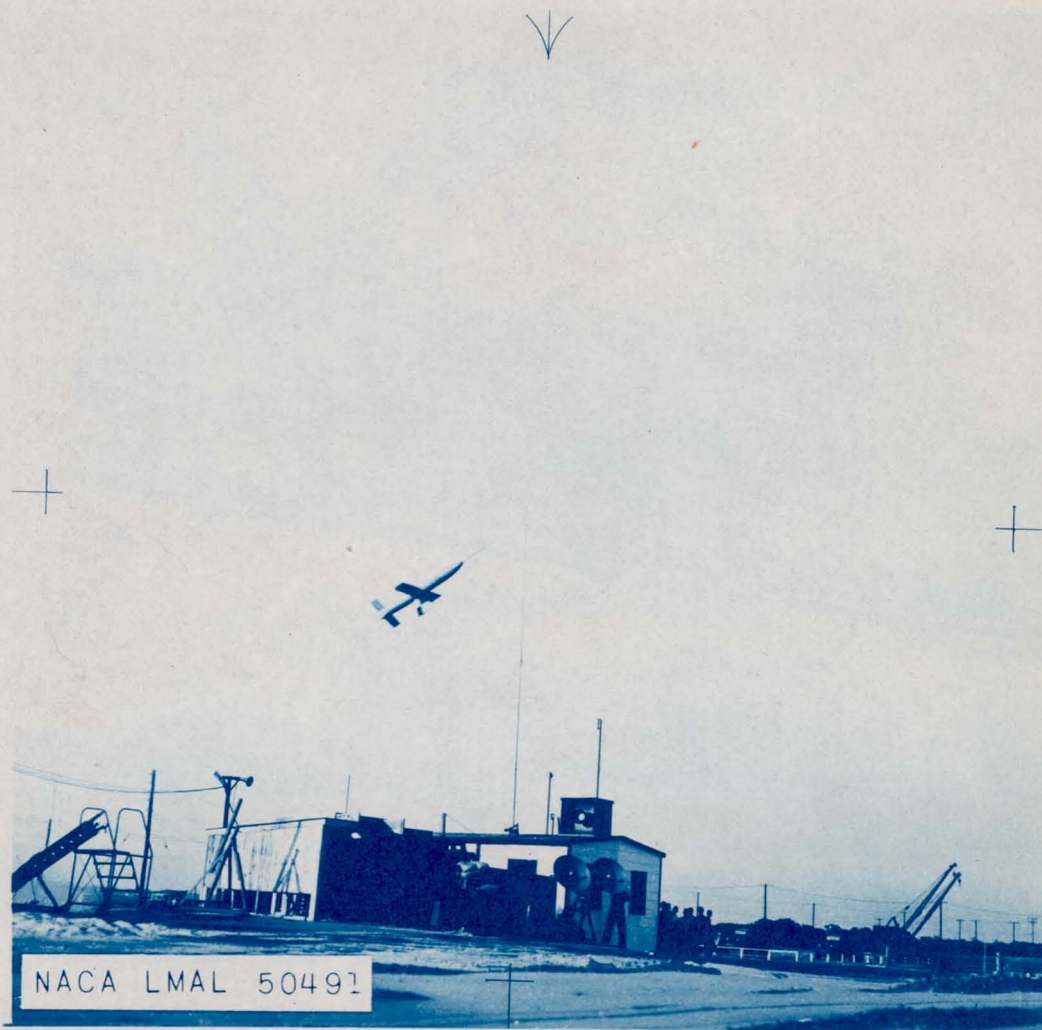


Figure 8.- Launching of model Lark; standard configuration; $\delta_f = 60^\circ$.

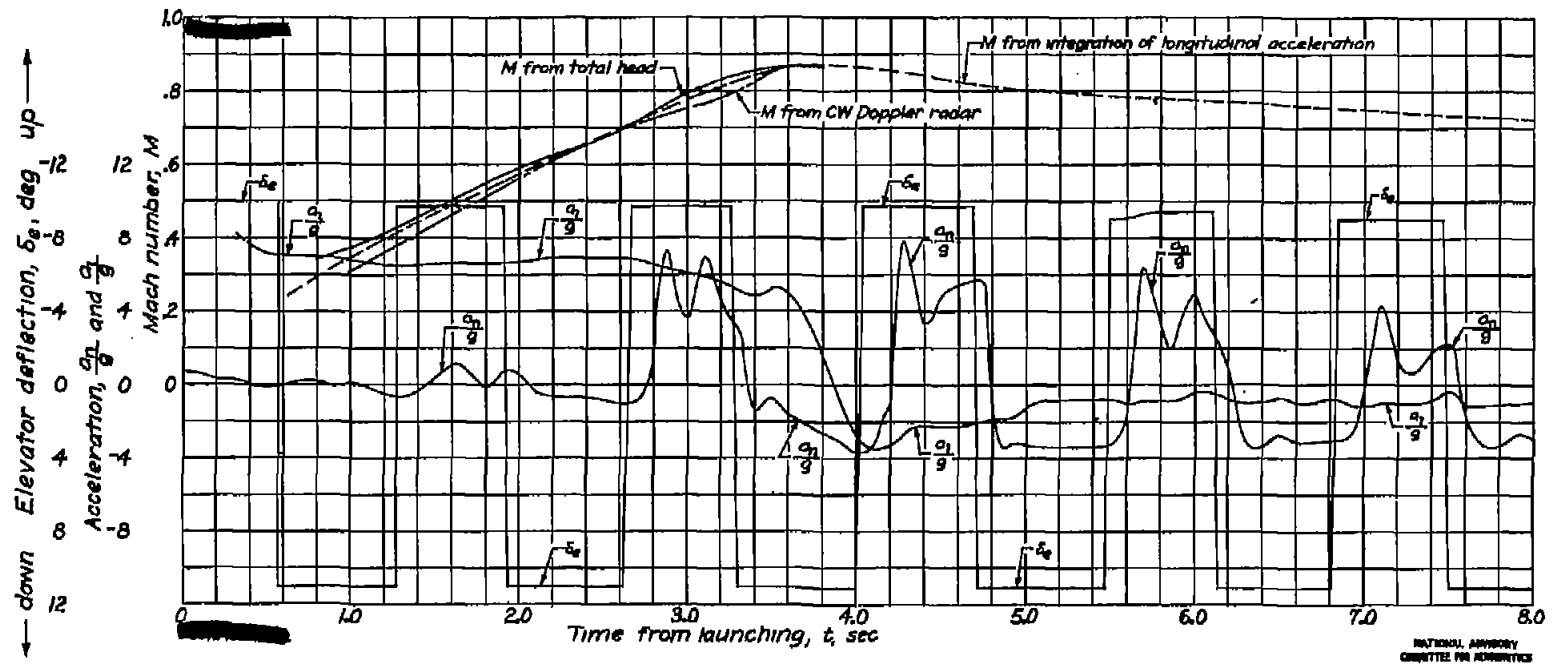


Figure 9.- Variation of Mach number, elevator deflection, and normal and longitudinal accelerations with time. Model with tail in line with wings; $\delta_f = 0$.

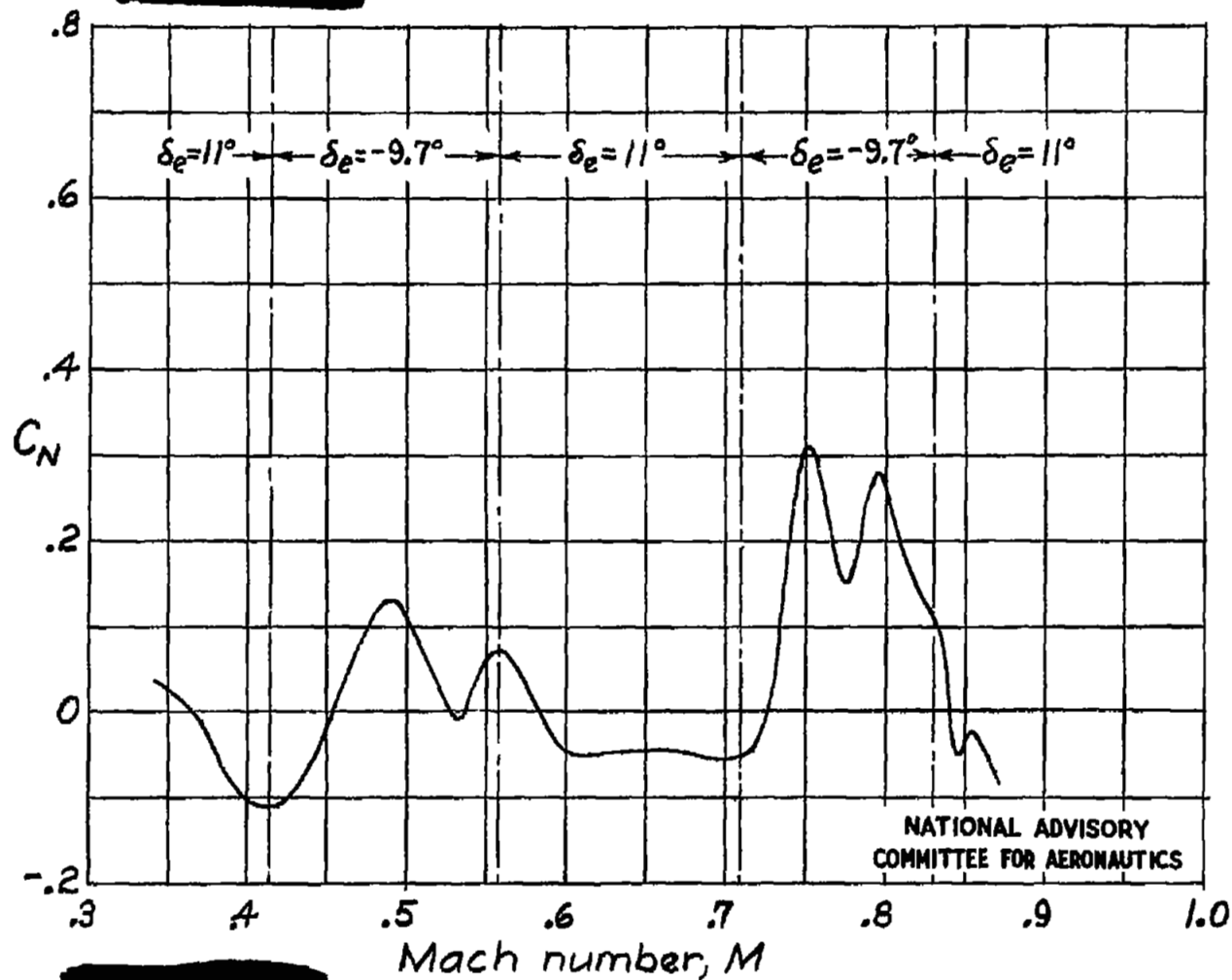


Figure 10. - Variation of normal-force coefficient with Mach number for the power-on part of the flight. Model with tail in line with wings; $\delta_f = 0^\circ$.

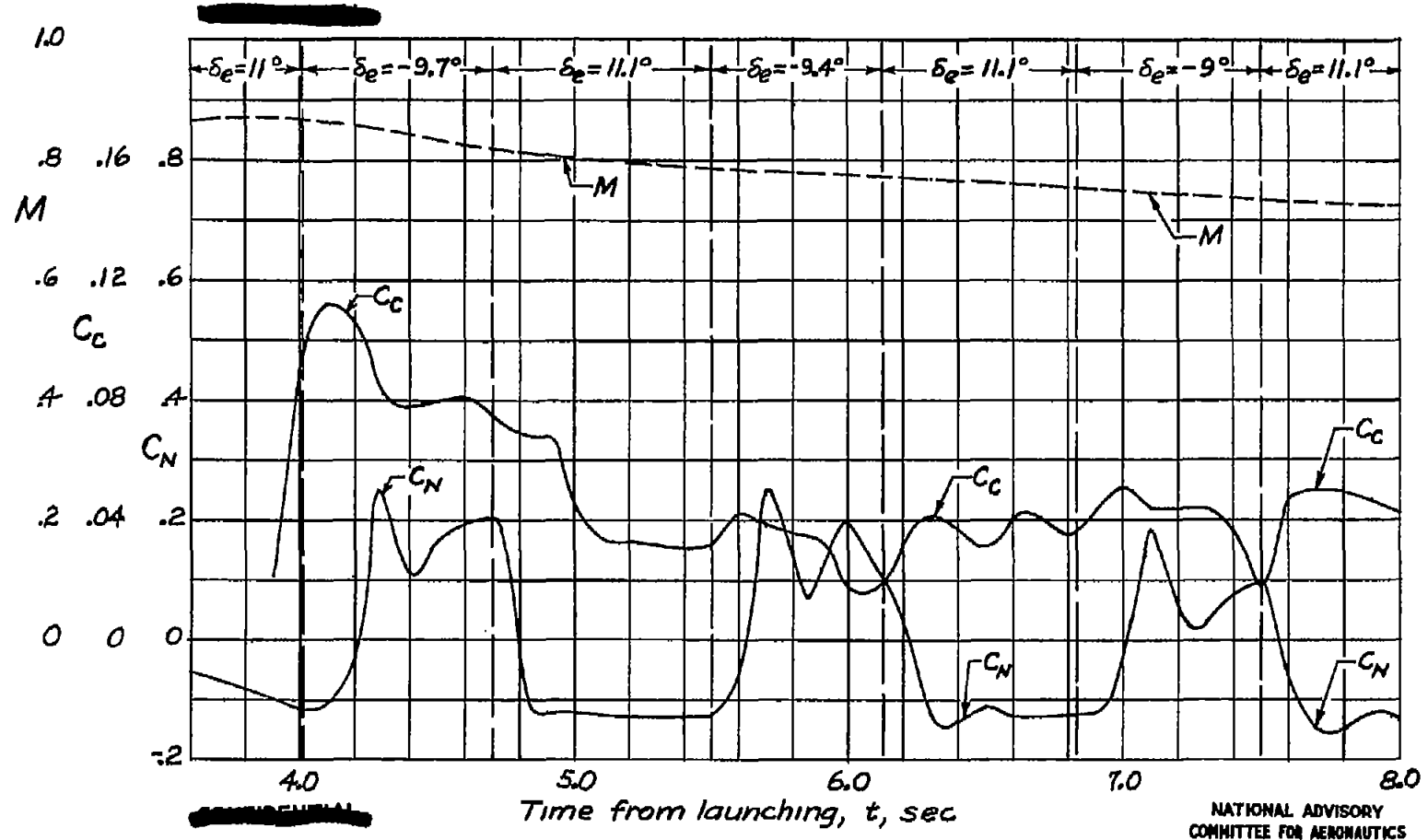


Figure 11.- Variation of Mach number and chord-force and normal-force coefficients with time for the power-off part of the flight. Model with tail in line with wings; $\delta_p = 0^\circ$

NATIONAL ADVISORY COMMITTEE FOR AERONAUTICS

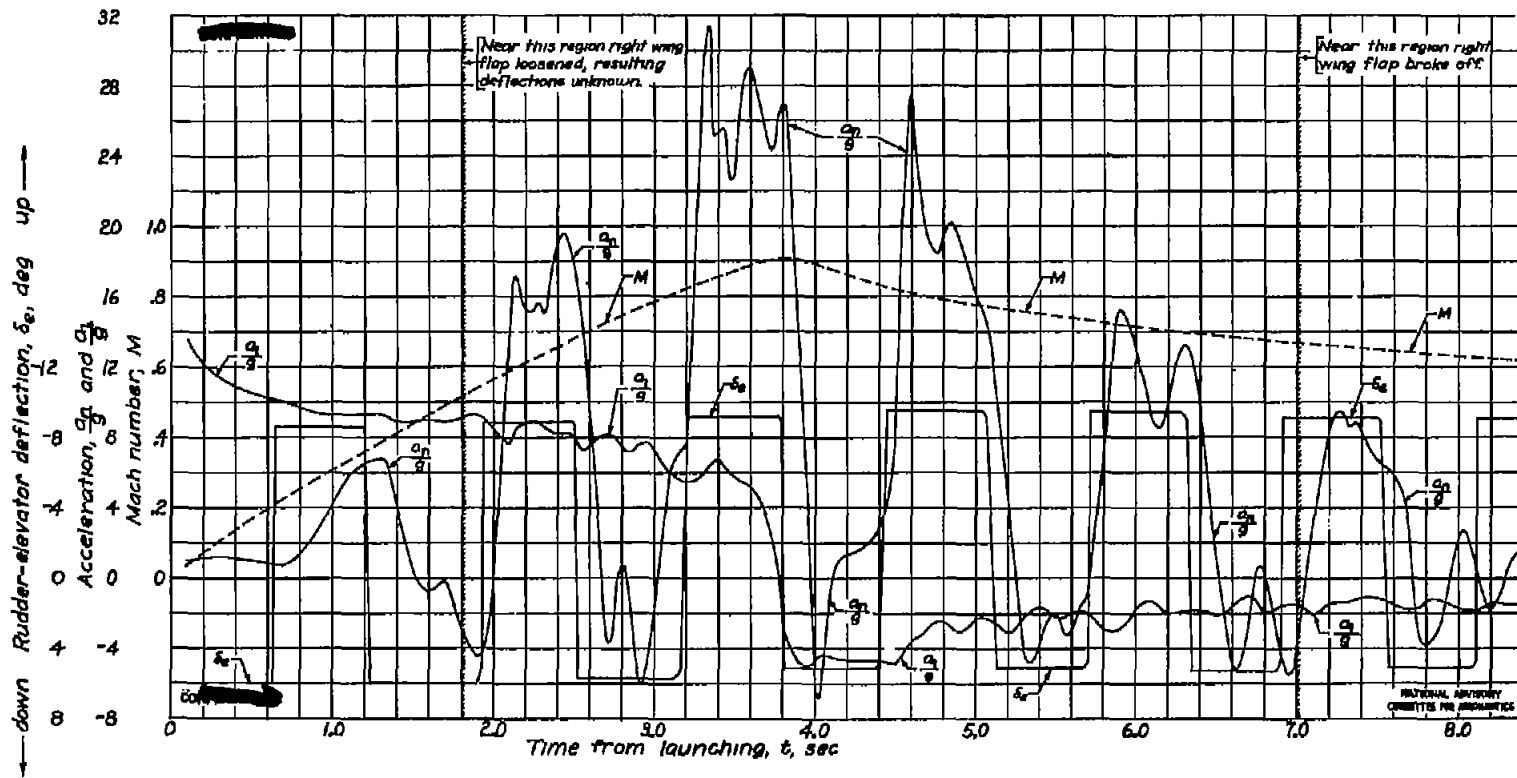


Figure 12.- Variation of Mach number, rudder-elevator deflection, and normal and longitudinal accelerations with time. Model of standard configuration; $\xi_f = 60^\circ$

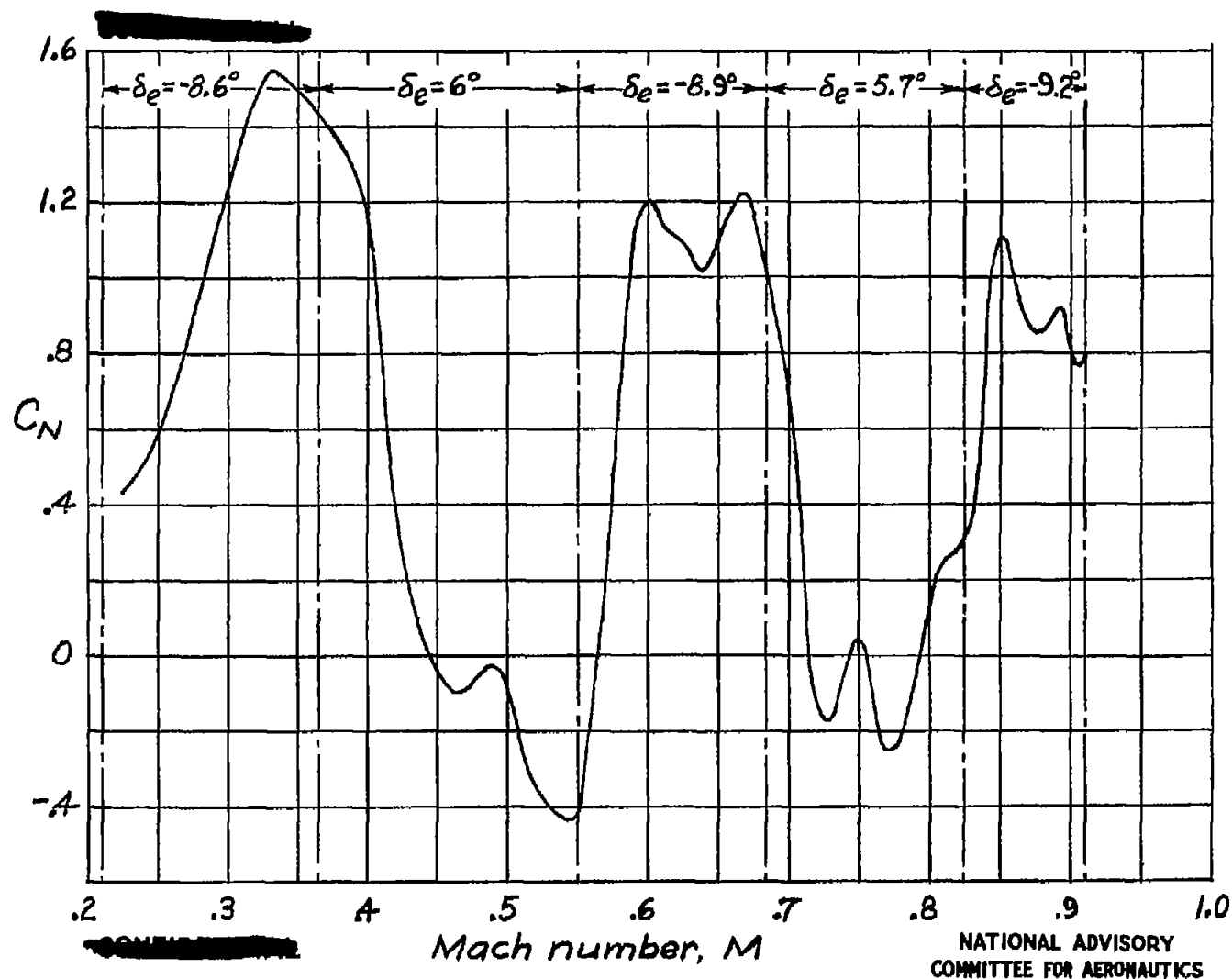


Figure 13.- Variation of normal-force coefficient with Mach number for the power-on part of the flight. Model of standard configuration; $\xi_f \approx 60^\circ$

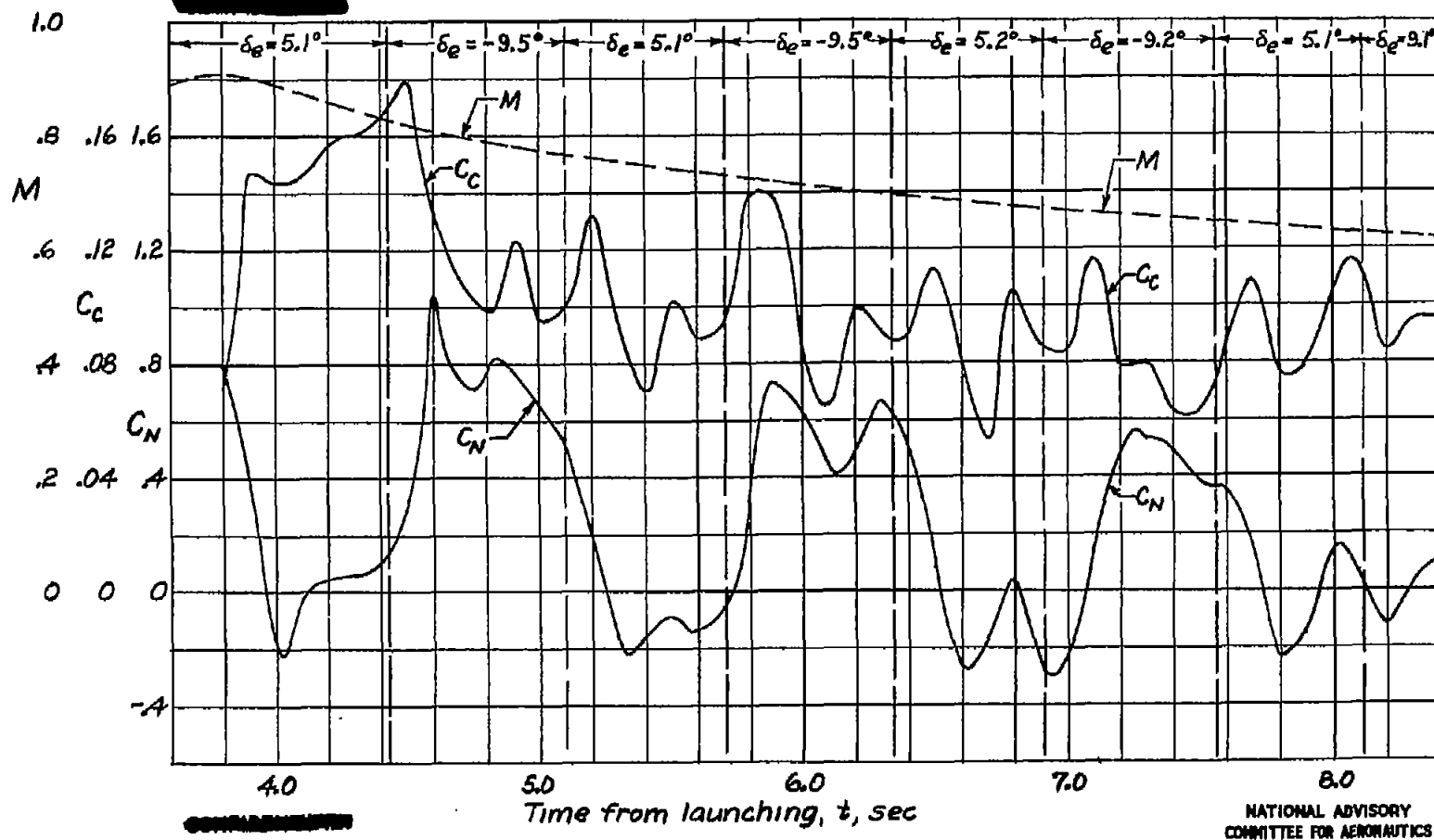


Figure 14.- Variation of Mach number and chord-force and normal-force coefficients with time for the power-off part of the flight. Model of standard configuration; $\delta_F \approx 60^\circ$.

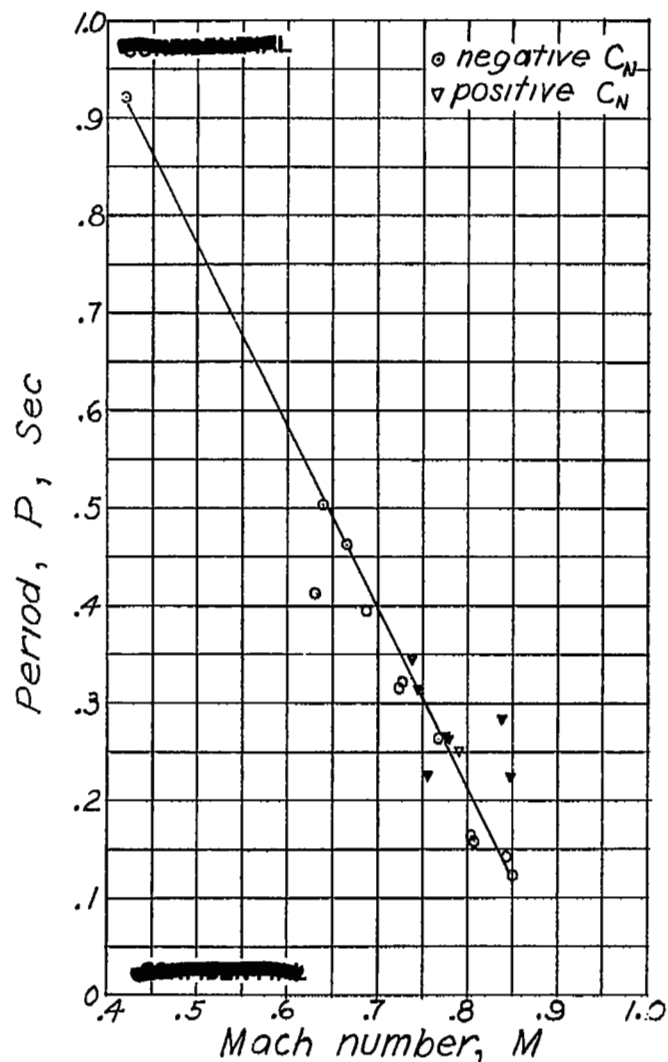
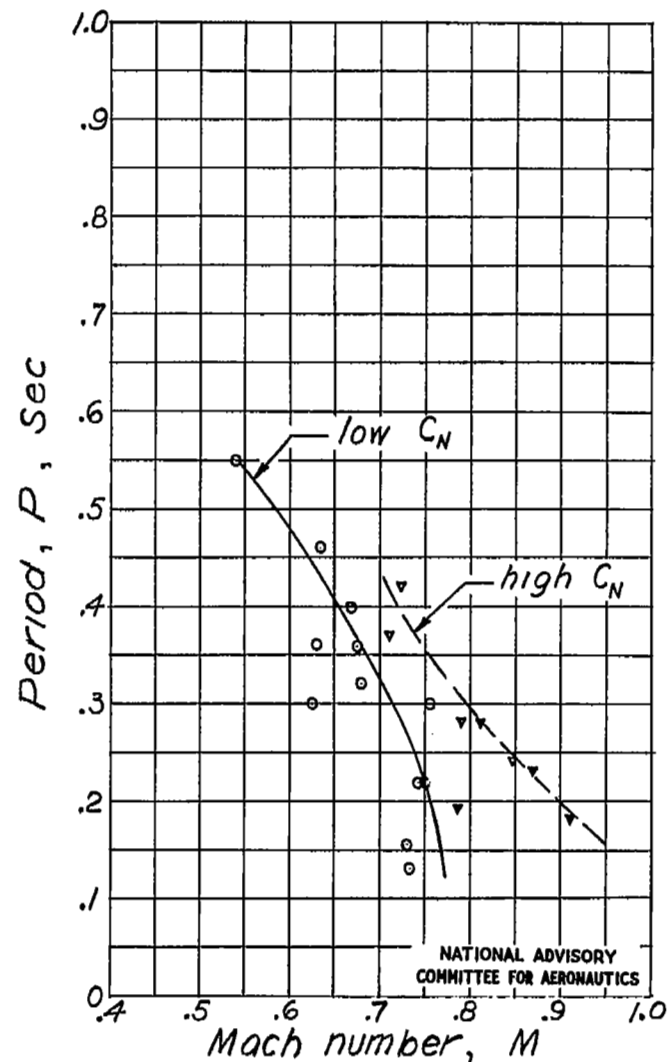
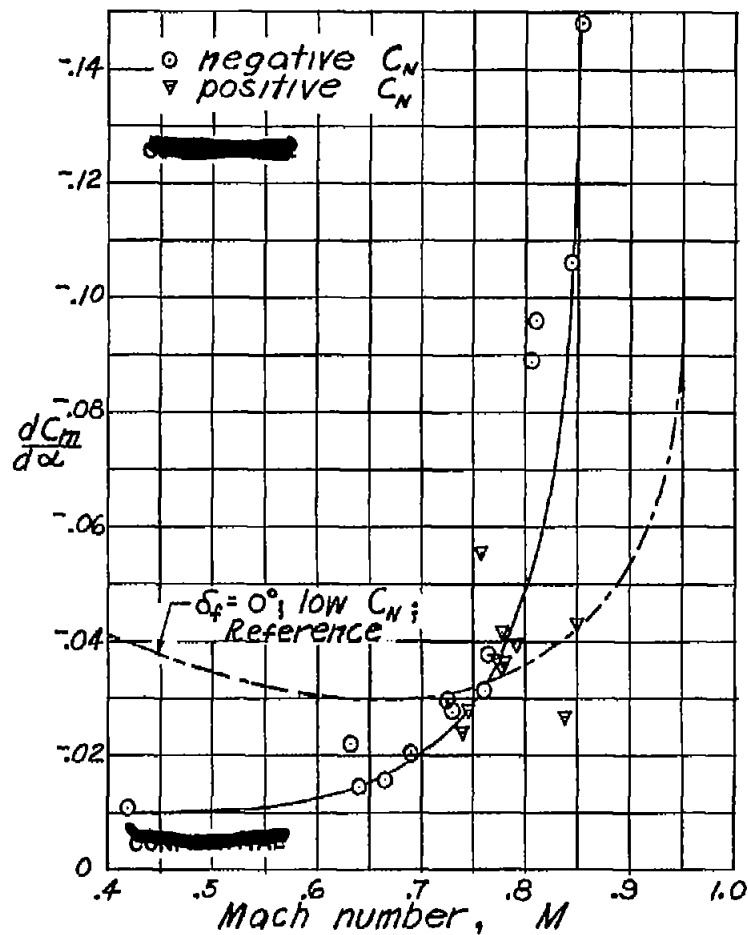
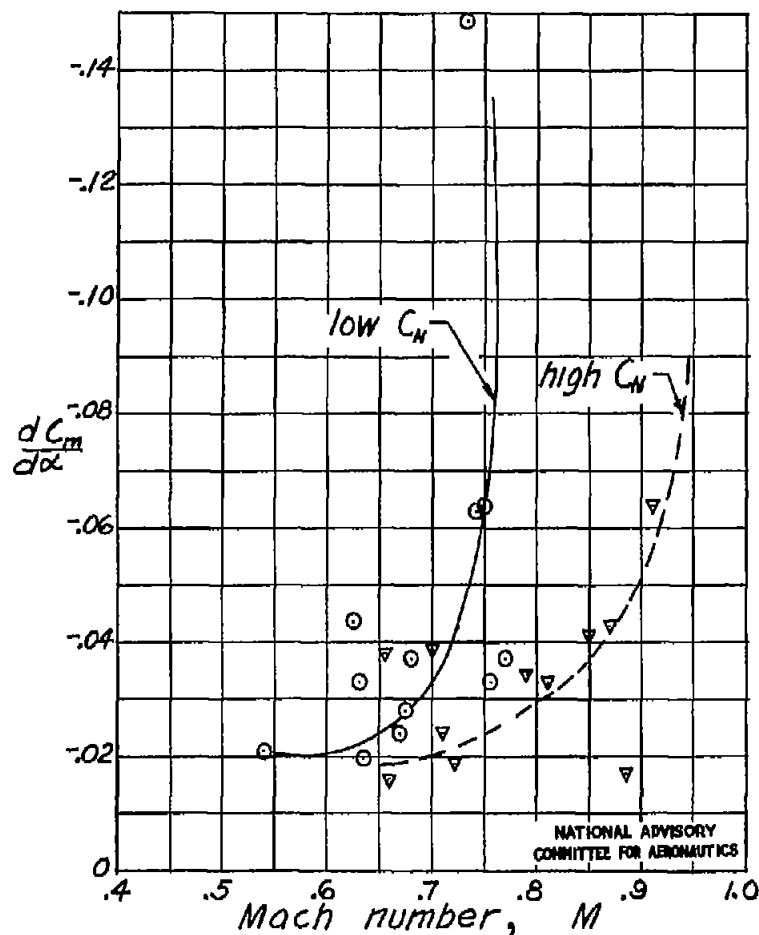
(a) Tail in line ; $\delta_f = 0^\circ$ (b) Standard configuration ; $\delta_f \approx 60^\circ$

Figure 15.- Variation of the period of the short-period oscillation with Mach number.



(a) Tail in line ; $\delta_f = 0^\circ$



(b) Standard configuration ; $\delta_f \approx 60^\circ$

Figure 16.- Variation of the static longitudinal stability with Mach number.

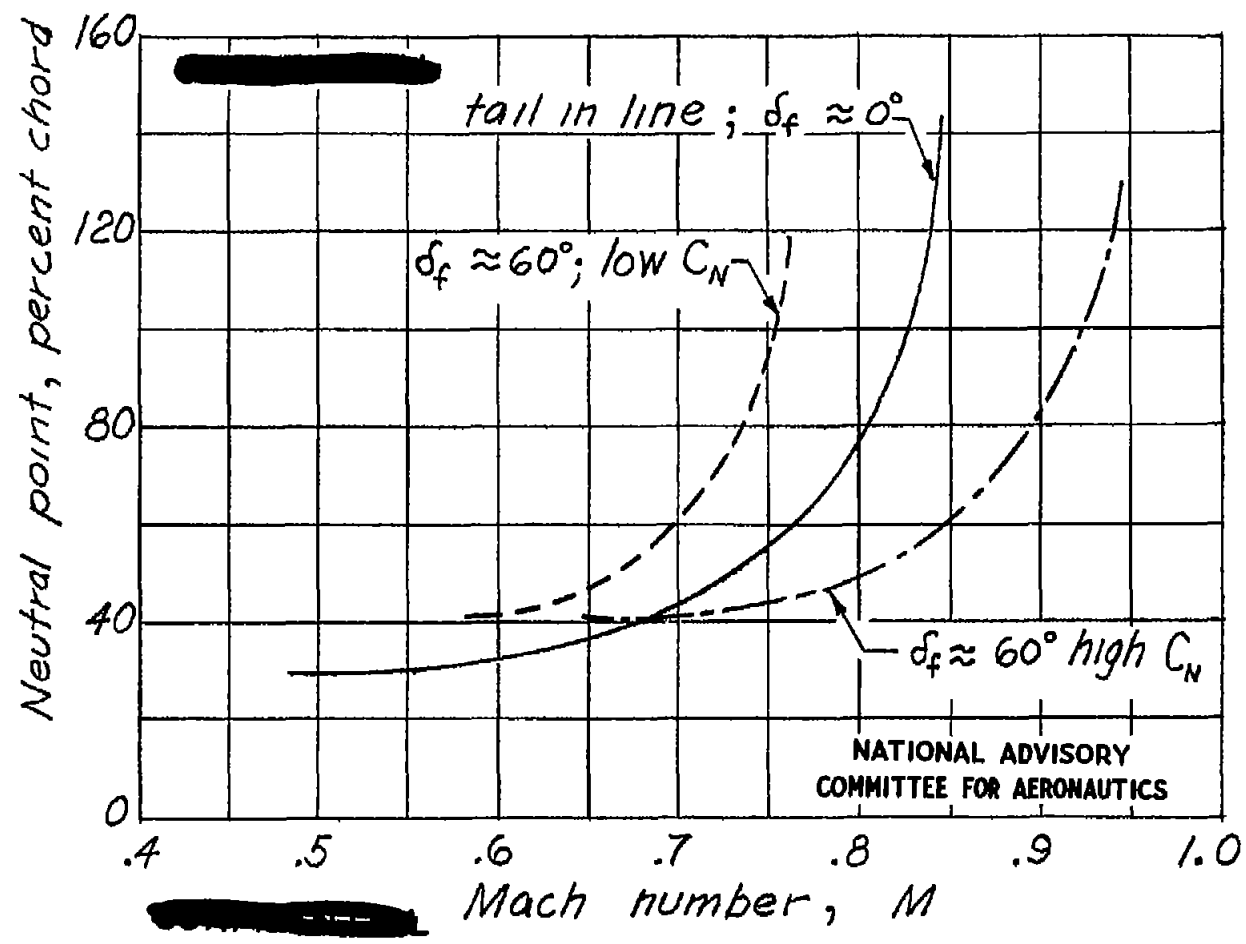


Figure 17. - Variation of the neutral point with Mach number; $\frac{dC_L}{d\alpha}$ assumed to be 0.08.

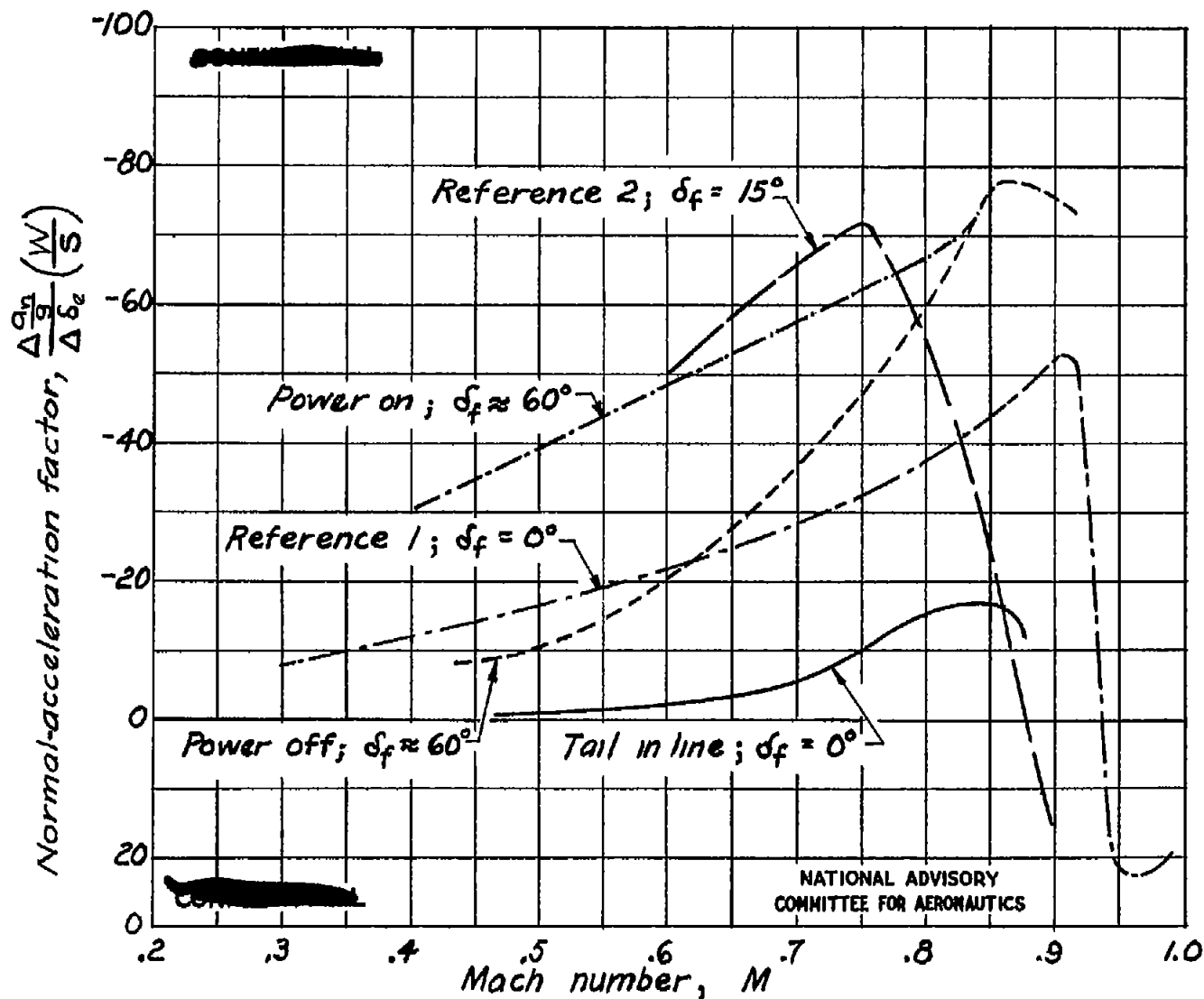


Figure 18.- Comparison of the normal acceleration producing ability of the control surfaces for all the configurations.